Polymer 206 (2020) 122862

Contents lists available at ScienceDirect

Polymer

journal homepage: http://www.elsevier.com/locate/polymer

Enhanced self-healing performance of graphene oxide/vitrimer nanocomposites: A molecular dynamics simulations study

Chanwook Park [a], Geonwoo Kim [a], Jiwon Jung [a], Balaji Krishnakumar [c], Sravendra Rana [c,**], Gun Jin Yun [a,b,*]

[a] Department of Mechanical & Aerospace Engineering, Seoul National University, Seoul, 08826, South Korea
[b] Institute of Advanced Aerospace Technology, Seoul National University, Gwanak-gu, Gwanak-ro 1, Seoul, 08826, South Korea
[c] University of Petroleum & Energy Studies (UPES), School of Engineering, Energy Acres, Bidholi, Dehradun, 248007, India

ARTICLE INFO

Keywords:
Vitrimer
Molecular dynamics
Self-healing
Graphine oxide
Nanocomposites

ABSTRACT

In this paper, we elucidate the filler effect of the vitrimer nanocomposites in the atomistic aspect for the first time with the molecular dynamics (MD) simulations. The self-healing properties are compared between GO/vitrimer nanocomposites and pristine vitrimers by the self-healing simulation containing the bond exchange reaction algorithm. The results reveal that GO reduces the vitrimers' T_g as well as the nanocomposites self-heal better than the vitrimers at all temperature ranges: temp. higher than T_g of both, temp. between the two T_g s, and temp. lower than T_g of both. Atomistic investigations demonstrate that the number of new disulfide bonds that emerged during the self-healing simulation increases in GO/vitrimer nanocomposites, which corroborates adding GO into the vitrimer stimulates the bond exchange reaction. Moreover, our simulation results imply that diverse nano-fillers can be adopted for the same purpose.

1. Introduction

Associative covalent adaptable network polymers, also known as vitrimers, are gaining enormous research interest in that it can replace conventional non-recyclable thermosetting polymers in various academic and industrial fields [1–10]. Various types of vitrimer chemistry have been reported such as transesterification [1–5], transalkylation [6], transamination [7,11,12], and disulfide [8,9] where it is generally known that their rate of dynamic bond exchange shows an Arrhenius-like temperature dependence.

Typical features of vitrimers encompass self-healing, reprocessing, and recycling which has never been possible with classical thermoset materials [13–15]. The self-healing, often related to the reprocessing, is enabled by introducing reversible crosslinks into the epoxy network. For example, Canadell et al. [8] demonstrated the self-healable thermoset epoxy network by introducing reversible disulfide groups that activate upon heating. They reported a broken tensile specimen fully recovers its tensile strength only in 1 h at 60 °C. Post et al. [16] further extended this chemical system to the fiber-reinforced composites, introducing a glass fiber-reinforced thermoset epoxy system containing disulfide bonds. By a thermal process for 16 h at 85 °C, the interlaminar fracture toughness was fully recovered while the tensile strength is recovered by 80%.

Recently, both experimental and simulation studies on vitrimers that can be dissolved in organic solvent have been reported and the fully-recyclable carbon fiber reinforced composites (CFRC) are expected to be commercialized in the near future [11,12,17–20]. For example, Yu et al. [17] demonstrated a fully-recyclable CFRC made of vitrimer and carbon fiber woven fabric utilizing their finding that the transesterification-type vitrimer can be decomposed in ethylene glycol solvent. Yang et al. [20] took one step further to simulate the governing process of the decomposition of the vitrimer under the ethylene glycol solvent by using molecular dynamics (MD) simulations. The authors also studied how the solvent size affects the dynamics of the vitrimer decomposition. However, this vitrimer chemistry entails catalysts, which make the manufacturing process complicated and might reduce the dynamics of bond exchange reaction (BER) upon repeated recycling. Taynton et al. [12] developed a catalyst-free transamination-type vitrimer that can be fully dissolved in an organic solvent containing amine groups (e.g., excess diamine monomer) at an ambient condition. This new material was used for the matrix phase of the CFRC and exhibited

* Corresponding author. Department of Mechanical & Aerospace Engineering, Seoul National University, Seoul, 08826, South Korea.
** Corresponding author.
E-mail addresses: srana@ddn.upes.ac.in (S. Rana), gunjin.yun@snu.ac.kr (G.J. Yun).

https://doi.org/10.1016/j.polymer.2020.122862
Received 23 June 2020; Received in revised form 16 July 2020; Accepted 26 July 2020
Available online 12 August 2020
0032-3861/

perfect recyclability; pristine carbon fibers were recovered from a fully cured CFRC.

Since the dynamic crosslinked network is frozen at ambient temperature, it is believed that vitrimers behave like thermosetting polymers under this condition, both chemically and mechanically [21]. However, although they maintain the crosslinked structure in such conditions, their mechanical properties are weaker than conventional thermosetting polymers (e.g., epoxy resin) [12]. To enhance the mechanical properties of vitrimers, several nanofillers have been used as reinforcing fillers [21,22]. For instance, Legrand et al. [21] added silica nanoparticles into a transesterification-type vitrimer and obtained silica/vitrimer nanocomposites with filler contents up to 40 wt% under large scale and solvent-free conditions. The authors observed that the mechanical properties of vitrimer nanocomposites are enhanced upon the filler contents. Especially when the silica fillers are functionalized with epoxide groups, the functionalized fillers participate in the BER of the vitrimer so that both the interfacial interaction and the dispersion are improved. Krishnakumar et al. [22,23] confirmed that adding graphene oxide (GO) into a disulfide-type vitrimer enhances its mechanical properties and more interestingly, the self-healing properties. Pristine vitrimer and GO/vitrimer nanocomposite (1.0 wt%) recovered 73% and 88% of their flexural modulus at the first healing and 60% and 80% of their flexural modulus at the second healing, respectively [22]. They attributed this result to the reduced T_g of GO/vitrimer nanocomposites but left a detailed atomistic interpretation for future work.

In this study, with the aid of MD simulations, the disulfide BER is realized by the devised BER algorithm. This algorithm is exploited to directly compare BER and self-healing characteristics of GO/vitrimer nanocomposites and pure vitrimers. For this purpose, a self-healing simulation containing a series of cut-BER(healing)-tension is proposed with a protocol for an assessment of the self-healing performance. This work is the first one to use MD simulations to investigate the GO filler effect on vitrimer nanocomposites. Our simulation results suggest a valid explanation for the GO filler effect of vitrimer nanocomposites in the atomic scale and the possibility of using diverse nanofillers for the same purpose.

2. Molecular dynamics simulations

Initial molecular structures such as epoxy resins (Diglycidyl ether bisphenol A, DGEBA) and hardener (2-Aminophenyl disulfide, AFD) were generated in the Materials Studio 2017 package[1]. The initial structures were then converted to large-scale atomic/molecular massively parallel simulator (LAMMPS) [24] data files for further MD simulations. The all-atomic MD simulations were performed under the polymer consistent force field (PCFF) [25], which has been extensively adopted for polymeric nanocomposits [26–30]. For the non-bonded potentials (van der Waals and Coulomb interactions), a cutoff distance of 9.5 Å was used, and the Ewald summation method with an accuracy of 0.0001 kcal/mol was adopted [31]. Geometry optimization based on the conjugate gradient algorithm was performed with 10^{-4} (unitless) and 0.5 (Kcal/mol·Å) of energy and force tolerance, respectively. The temperature and pressure of NVT (constant number of atoms, volume, and temperature) and NPT (constant number of atoms, pressure, and temperature) ensembles were controlled using the Nose-Hoover thermostat and barostat, and a timestep of 1.0 fs was used during dynamics simulations [32,33]. Periodic boundary conditions were employed in all directions to overcome the size limit and eliminate surface effects. The OVITO program was used as a visualizer of LAMMPS dump files [34].

[1] BIOVIA, *Materials Studio*, 2017. Available from: http://www.3dsbiovia.com/.

2.1. Dynamic crosslink simulations

To build an MD model of vitrimer, an initial structure consisting of 296 DGEBA and 148 AFD molecules was generated. Reactive atoms in DGEBA and AFD were named as R1 and R2, respectively, as shown in Fig. 1(a). Then the dynamic crosslink simulation described in our previous paper [35] was conducted to make a crosslinked structure with a target crosslink density of 90%. The crosslinked unit cell comprises 18,056 atoms and is shown in Fig. 1(b).

2.2. Graphene oxide (GO) modeling

We built an atomic model of GO by following the X-ray photoelectron spectroscopy (XPS) analysis given in the literature [36]. Luo et al. calculated the atomic percentages of GO using XPS to find that their GO sample comprised 61.57% of carbon and 39.43% of oxygen atoms [36]. By considering chemical features of GO and the fact that epoxy and hydroxyl groups are formed in the basal plane while carboxyl groups are formed at the edge of GO [37], we determined that a single layer graphene (C594) shown in Fig. 2(a) is functionalized with 150 epoxy groups and 150 hydroxyl groups in the basal plane and 35 carboxyl groups at the edge. The generated GO (C594 O370) shown in Fig. 2(a) achieved 38.38% of oxygen atoms. It was then packed with 296 DGEBA and 148 AFD (same as the vitrimer model) and went through the dynamic crosslink simulation with a target density of 90%. The generated GO/vitrimer model is illustrated in Fig. 2(b).

It is important to note that we did not crosslink between the functional groups in GO and the epoxy matrix; only non-bonded interactions were considered at the interface. This is because in our preceding experimental paper [22] – the target material system of this study – no clues have been found that the GO is crosslinked with the vitrimer matrix, from various characterizations such as FTIR, x-ray diffraction spectroscopy, and ultraviolet spectroscopy.

2.3. Bond exchange reaction (BER) algorithm (BER loop)

The BER in the covalent adaptable network takes place simultaneously, where a new bond is created in exchange for breaking the existing bond. To model this bond-swapping network, a bond swap method has been developed with a three-body coarse-grained potential [38]. In this method, the energy gain at a bond formation offsets the energy loss from the three-body potential with a tunable model parameter [39]. In this study, however, we adopt the all-atomistic PCFF force field to scrutinize the disulfide-type vitrimer nanocomposite systems containing DGEBA resin, AFD hardener, and GO. Furthermore, the current technology of all-atomistic MD simulations is incapable of realizing the bond swap method with the novel three-body potential in an existing force field such as PCFF. Instead, only successive breaking/creation command is available during the dynamics simulations [40,41]. This is the reason we devised an algorithm that can break and recreate disulfide bonds repeatedly during a dynamics simulation, as illustrated in Fig. 3(a).

The initial structure first goes through a short NPT ensemble dynamics for 10,000 steps to make sure its stability. Then it enters into two 'for loops'; disulfide bond breaking and bond creation, where we set two variables, "*a*": loop count of bond breaking, and "*b*": loop count of bond creation. That is, once 80% of existing disulfide bonds are broken, two reactive sulfur atoms closer than a predefined cutoff distance (9 Å) are created with a probability of 50% at every 10,000 steps. The reason for choosing 10,000 steps of interval and 50% of probability is to avoid a self-break/creation. If every couple of sulfur bonds makes a disulfide bond in a short time interval, the same disulfide bond will be generated again before they are broken (see supporting video 1, BER conducted with 50% of bond creation probability and 2000 steps of an interval). However, with a longer time interval (10,000 steps), we were able to observe a new generation of disulfide bonds as illustrated in Fig. 3(b)

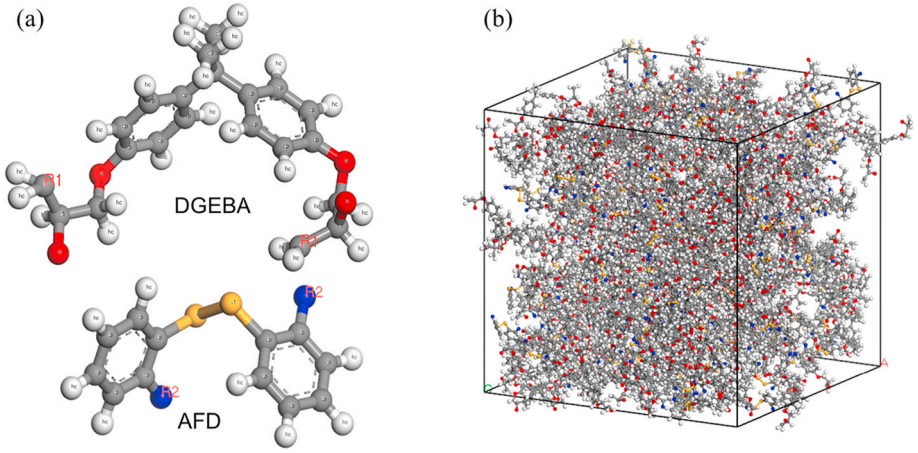

Fig. 1. (a) Atomistic model of DGEBA and AFD. The epoxide rings in the DGEBA are open and the both end carbon atoms are named as R1. Nitrogen atoms in the AFD are named as R2. (b) Crosslinked unit cell and the initial structure of vitrimer. (Color online). (For interpretation of the references to color in this figure legend, the reader is referred to the Web version of this article.)

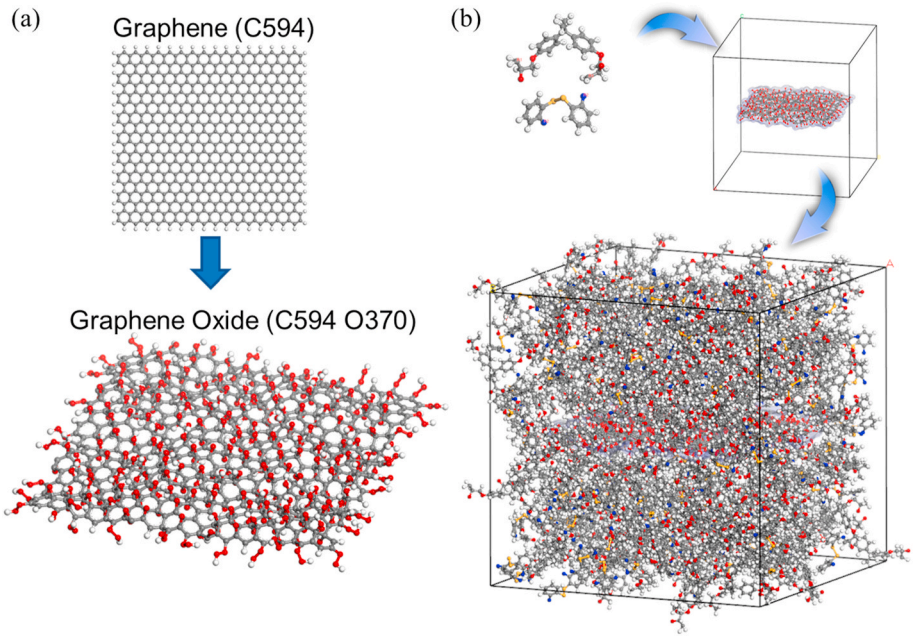

Fig. 2. (a) A single layer graphene (C594) is functionalized with epoxy, hydroxyl, and carboxyl groups to form a graphene oxide (C594 O370). (b) Initial structure of GO/vitrimer. A unit cell containing the GO is packed with the DGEBA and AFD molecules followed by the dynamic crosslink simulations to form a crosslinked structure having the same crosslink density with vitrimer models. (Color online). (For interpretation of the references to color in this figure legend, the reader is referred to the Web version of this article.)

and supporting video 2. It is worth noting that the probabilities of bond break and creation are set as 80% and 50%, respectively. Like the way of choosing the time interval as 10,000 steps, these probabilities are arbitrarily chosen to facilitate the BER. Since this study aims to compare the self-healing performance of GO/vitrimer and vitrimer under the same condition, these settings are maintained throughout the self-healing simulations.

2.4. Self-healing simulations

Now, by using the BER algorithm, we can conduct a self-healing simulation consisting of cut, BER loop (healing), and tension. MD tensile simulations have been widely conducted and we follow a universal method for the dynamic uniaxial tensile test described in our previous paper [42,43]. We adopt a strain rate of $2 \times 10^9/s$ throughout tensile simulations. However, before we finalize the self-healing simulation protocol, we need to define the cutting range and maximum loop counts.

2.4.1. Defining cutting range

In LAMMPS, the bond breaking is available via the fix bond/break command. It can break specified bonds in a group of atoms. To cut in the middle of an MD unit cell, we delete every backbone bond in the vitrimer system. However, the thickness of the group that we are going to delete backbone bonds is unknown, as illustrated in Fig. 4(a). Therefore, we conducted cut-tension simulations with different thickness of the cutting range, 2 Å and 3 Å. As seen in Fig. 4(b), the 2 Å-thick cutting range is incomplete. The stress level of the stress-strain curve does not approach zero and extended backbone chains are observed in the snapshot at an engineering strain of 1.0. On the other hand, when the cutting thickness is 3 Å (Fig. 4(c)), the stress level approaches zero and we can observe a clear cut in snapshots taken at engineering strains of 0.4 and 1.0. Therefore, the thickness of 3Åwas adopted throughout the self-healing simulations.

2.4.2. Defining maximum loop counts

The last thing that should be determined for the self-healing simulations is the maximum loop counts, "*a*" and "*b*" in Fig. 3(a). The max of

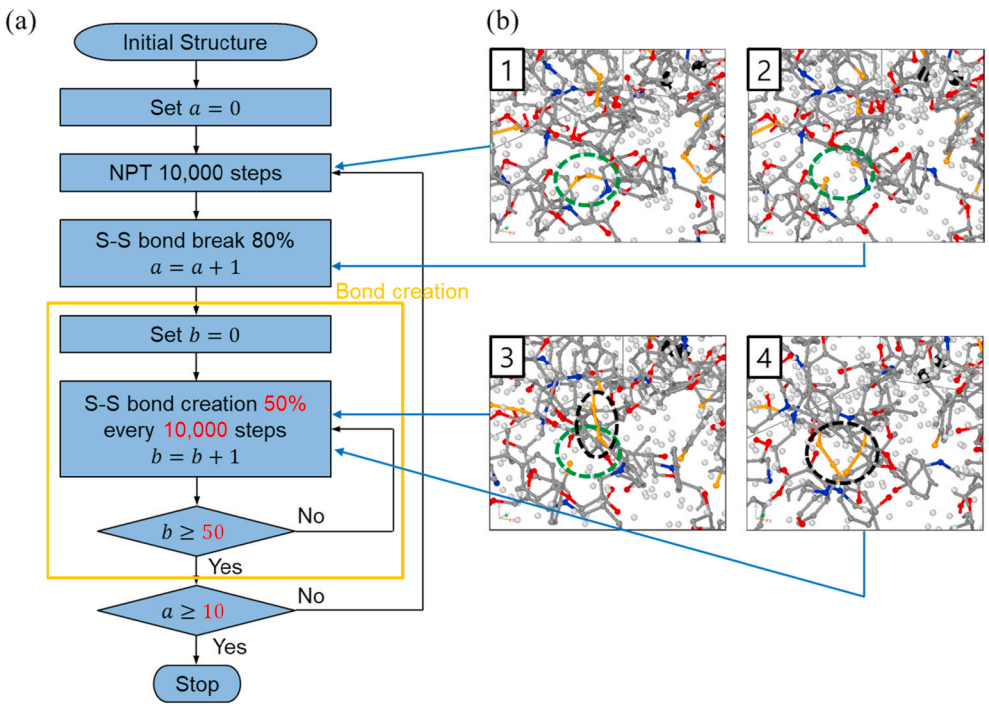

Fig. 3. (a) Bond break/create algorithm. Red numbers are to be determined. (b) Screen shots of the BER loop with 50% of bond creation probability and 10,000 steps of time interval. Atoms are colored in the following description: sulfur-orange, carbon-gray, oxygen-red, hydrogen-white. (on-line version can distinguish the colors). 1: A disulfide bond is in the green dotted circle. 2: The disulfide bond is broken. 3: The right-hand side sulfur atom creates a bond with another sulfur atom outside the green dotted circle; new disulfide bond is in the black dotted circle. 4: The left-hand side sulfur atom creates a new disulfide bond with another sulfur atom; new disulfide bonds are now in the black dotted circle. (Color on-line). (For interpretation of the references to color in this figure legend, the reader is referred to the Web version of this article.)

loop count "*a*" means the total number of bond cuts throughout the BER loop while the max of loop count "*b*" means the total number of bond creations once the bonds are cut. Briefly, if the max of "*a*" and "*b*" increases, the total BER time step increases which corresponds to the healing time in the experiment. For instance, if the "*b*" max is set as 10, the bond creation loop will run for 100,000 steps (100 ps in the time domain). Then if the "*a*" max is 10, the total BER loop will run for 1,000,000 steps (1 ns in the time domain). It is obvious that higher "*a*", "*b*" max values result in longer simulation time, that is, longer healing time. Thus we should define an optimal "*a* ", "*b*" max values for further study. Fig. 5 shows stress-strain curves and snapshots at engineering strains of 0.4 and 0.8 (or 1.0) of self-healing simulations conducted under different max "*a* ", "*b*" values. We fixed the "*a*" max as 10 and varied the "*b*" max from 10 to 50. When the "*b*" max is 10, 30, and 40, the stress-strain curves go to near-zero stress level at the high strain level. On the other hand, when the "*b*" max is 50, the stress level does not reach zero and the snapshots at engineering strains of 0.4 and 0.8 show self-healed behavior. Therefore, we set "*a*", "*b*" max values as 10 and 50, respectively and the total simulation time for the BER loop is 5 ns?

Now, we have finalized the self-healing simulation conditions. The BER algorithm in the self-healing simulation adopts iterative bond breaking/creation loops, resulting in a fixed BER simulation time. However, this does not guarantee the number of disulfide bonds remains constant during the BER, which is the chemical feature of vitrimers. Therefore, we need to discuss the possible fluctuation of the number of disulfide bonds. Fig. 6 shows the number of disulfide bonds of GO/vitrimer and vitrimer during the 5ns of the BER loop. As expected, the number of disulfide bonds fluctuates as the BER loop progresses. However, no clear trend (ascent or descent) is observed as the loop count (or the simulation time) increases and the fluctuation is marginal: typical values reside in 137–141. Moreover, most of the gap between GO/vitrimer and vitrimer is less than the error bar. Therefore, we conclude that the fluctuation of the number of disulfide bonds can be neglected; the total number of disulfide bonds is maintained during the self-healing simulations.

3. Results and discussion

In this section, we compare the self-healing performance of GO/vitrimer and vitrimer models through the devised self-healing simulation and investigate results from the atomistic perspective. Since both models are given with the same self-healing condition, a direct comparison between the GO/vitrimer and vitrimer is available.

3.1. Glass transition temperature (T_g)

To determine the simulation temperature, two transition temperatures related to the viscoelastic behavior of vitrimers should be investigated: the glass transition temperature, T_g, and the topology freezing temperature, T_v. T_g is the temperature range where a transition from the glassy state to the rubbery state takes place. Unlike T_g that is a general characteristic of polymeric materials, T_v is a vitrimer-only characteristic temperature at which the timescale of BER becomes shorter than that of the deformation of materials, resulting in the rearrangement of the network topology and flow [2,44]. Theoretically, T_v can be higher than T_g or lower than T_g [44]. Whatever the case is, a visible self-healing occurs above the two transition temperatures since both the topology rearrangement and the segmental motion are the precondition for the self-healing. The experiments on the target material of this study confirmed that T_v and T_g are 19 °C and 64 °C, respectively [22]. Therefore, the temperature of self-healing simulations should be determined carefully according to T_g.

It is important to note that T_g calculations from MD simulations are not exactly the same as the experimental results due to the fast cooling down (or heating up) simulation conditions [27,45]. Because the theoretical transition from the glassy state to the rubbery state of MD models is defined by the T_g that is obtained from MD simulations, we first calculated the T_g. To avoid uncertainties derived from MD models, five different initial models of GO/vitrimer and vitrimer were generated where they share the same composition and crosslink density of their respective groups. Every simulation result is given with average values and error bars of three to five simulations conducted on different initial models.

The T_g was calculated by the cooling down method that was adopted

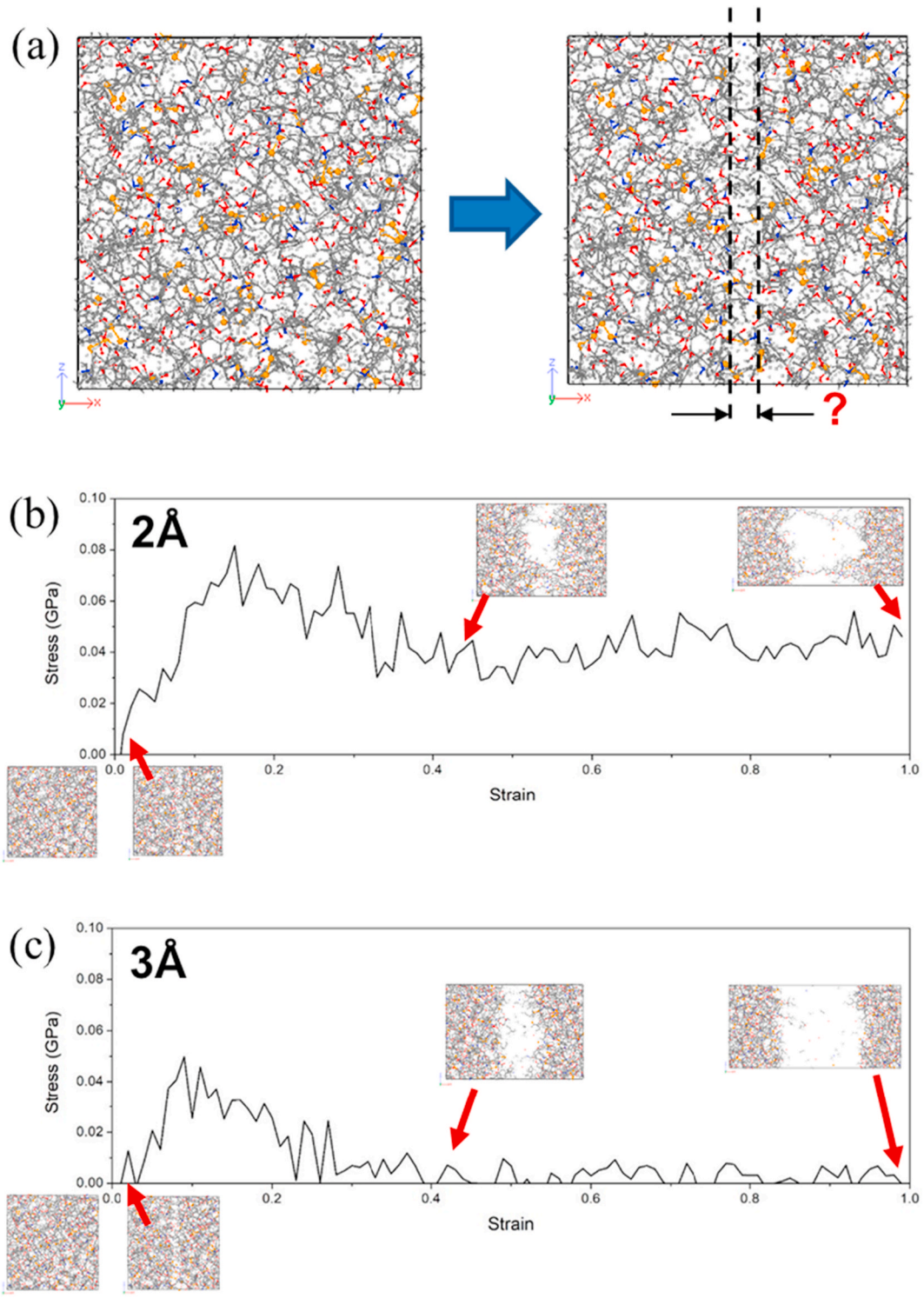

Fig. 4. Illustration of defining the cutting range (a). All backbone bonds of the vitrimer in the cutting range are deleted. Stress-strain curves and snapshots at engineering strain of 0, 0.4, and 1.0 when the cutting thickness is (b) 2 Å and (c) 3 Å. (Color online). (For interpretation of the references to color in this figure legend, the reader is referred to the Web version of this article.)

by our previous paper [27]. First, an MD model is equilibrated at 600 K. Then it is cooled down to 200 K with a cooling rate of 10^{11} K/ s. From the specific volume vs temperature graph shown in Fig. 7, we set T_g as the intersection point of the two linear fitted lines representing the glassy phase (200–400 K) and the rubbery phase (500–600 K). The T_g of GO/vitrimer was 20 K lower than that of the vitrimer. The T_g drop of nanocomposites is a general phenomenon observed from both experiments and simulations [22,46,47]. This is because the interfacial bonding between nanofillers and polymeric matrices is generally week [35]. Moreover, in an atomistic point of view, the interfacial van der Waals (vdW) excluded volume stimulates molecular motions in the interphase region [47]. The vdW excluded volume and the interphase region can be captured from the concentration profile in Fig. 8 where the peak in the middle (colored gray) indicates the GO and the

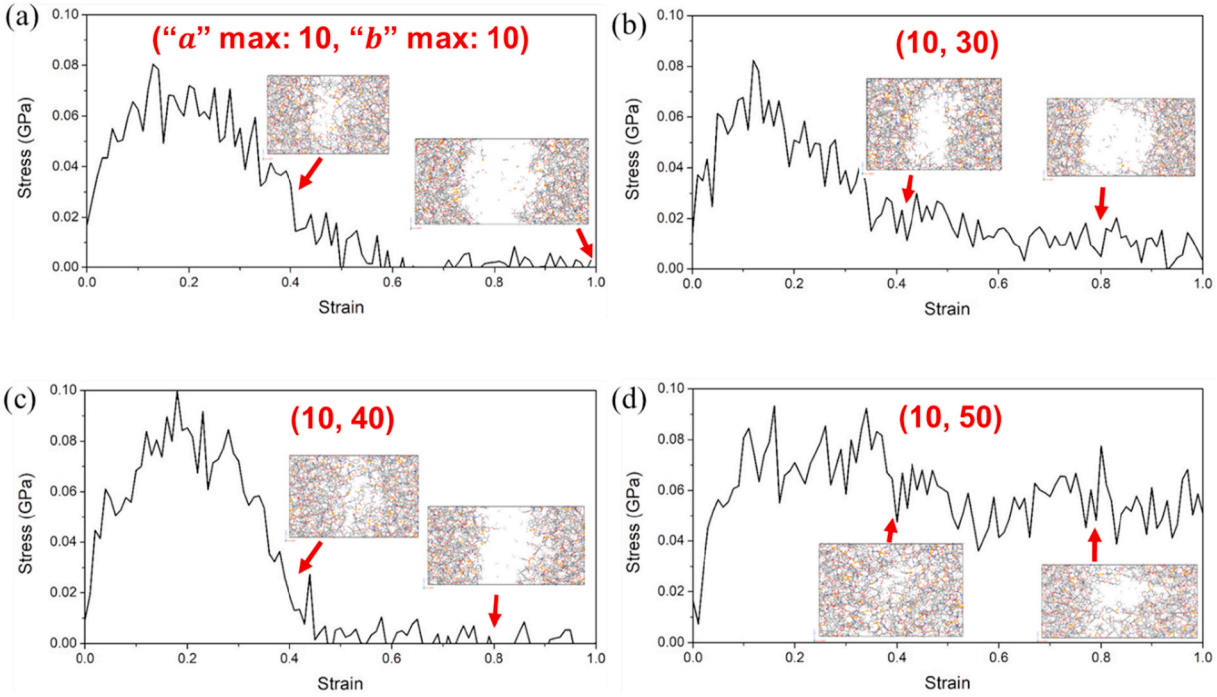

Fig. 5. Stress-strain curves and snapshots at engineering strain of 0.4 and 0.8 (or 1.0) of self-healing simulations conducted under different max "a ", "*b*" values. (a) "A" max:10, "*b*" max: 10. (b) "A" max:10, "*b*" max: 20. (c) "A" max:10, "*b*" max: 40. (d) "A" max:10, "*b*" max: 50. (Color online). (For interpretation of the references to color in this figure legend, the reader is referred to the Web version of this article.)

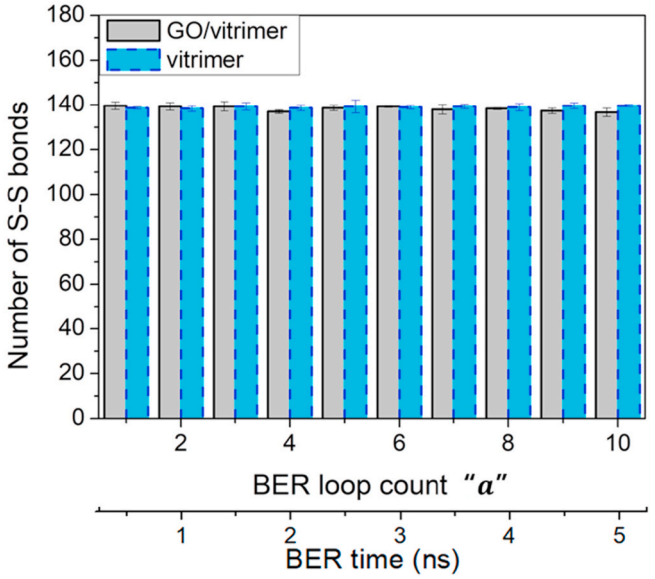

Fig. 6. The number of disulfide bonds as the BER loop count "*a*" increases at 400 K. Data from three different models are averaged in the plot with error bars. (Color online). (For interpretation of the references to color in this figure legend, the reader is referred to the Web version of this article.)

low-concentration regions (colored yellow) on both sides represent the vdW excluded volume. Note that the GO (thickness: 4.25 Å) is thicker than the single-layer graphene (thickness: 3.4 Å) [35] due to the functional groups on the basal plane. The interphase thickness is set as 8.5 Å, following our previous journal paper of GO/epoxy nanocomposites [35]. Because the regions of vdW excluded volume encompass a portion of the interphase matrix (due to the GO's warped morphology), the interphase region is defined as 8.5 Å-thick region next to the GO. The three regions – GO, vdW excluded volume, and interphase – characterized in Fig. 8 are used to discuss the interphase effect in Section 3.4.

From the calculated T_g, we set three simulation temperatures to compare the self-healing performance of GO/vitrimer and vitrimer; 400 K, higher than T_g of both models, 370 K, higher than T_g of GO/vitrimer but lower than T_g of vitrimer, 300 K, lower than T_g of both models.

3.2. Self-healing performance criteria

Before discussing the results of self-healing simulations, control groups – pure tension and cut-tension simulations – must be investigated. Fig. 9 shows stress-strain curves of the control groups conducted on GO/vitrimer and vitrimer models. The shapes of stress-strain curves of both models are similar to each other regardless of the simulation type; tension or cut-tension. In the case of tensile simulations, after the initial yield, stress-strain curves harden without showing any softening. In addition to this, the snapshots at the strain of 0.5 do not show large debonding and they maintain crosslinked structure at even higher strains. On the other hand, in the case of cut-tension simulations, stress-strain curves exhibit clear strain softening and the snapshots also manifest the large debonding at the cutting range in the middle of the model. That is, the crosslinked structure is no longer maintained near the cross-section. Especially in Fig. 9(c), the GO is completely pulled out at the strain of 1.0. From this analysis, we define the self-healing criteria that tells whether the self-healing is successful or not:

1. No softening in stress-strain curve
2. Maintain cross-linked structure at 0.5 strain (not showing large debonding)

If the result of a self-healing simulation satisfies the two criteria, one can say the self-healing is successful.

3.3. Self-healing simulations at 400 K, 370 K, and 300 K

Fig. 10 illustrates the results of self-healing simulations. Each figure is illustrated with stress-strain curves, snapshots at several strain levels

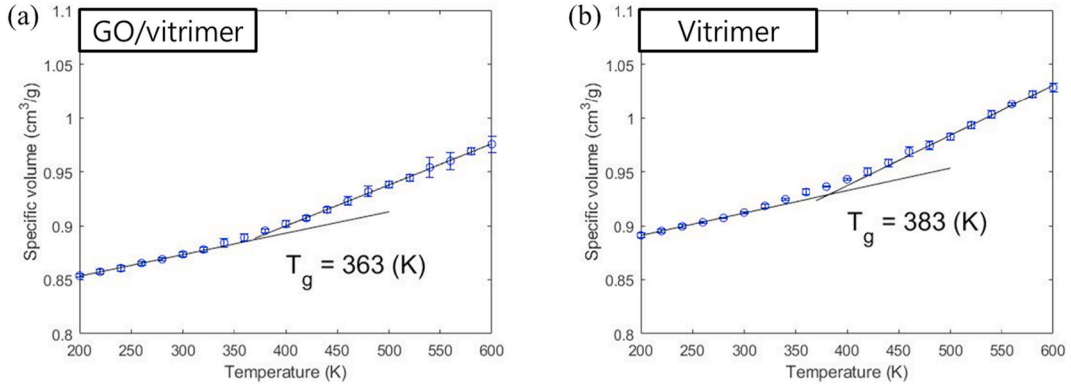

Fig. 7. Specific volume vs temperature graph of (a) GO/vitrimer and (b) vitrimer. Calculated T_g s of GO/vitrimer and vitrimer are 363 K and 383 K, respectively. (Color online). (For interpretation of the references to color in this figure legend, the reader is referred to the Web version of this article.)

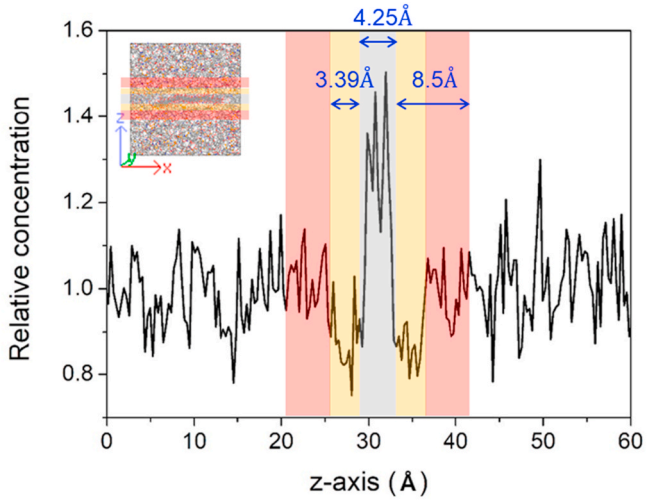

Fig. 8. Concentration profile along the z-axis. Gray and yellow regions represent the GO and vdW excluded volume, respectively. The interphase region is the 8.5 Å-thick region containing both yellow and red regions. The inset is a GO/vitrimer model divided by the three regions along the z-axis. (Color online). (For interpretation of the references to color in this figure legend, the reader is referred to the Web version of this article.)

(0, 0.5, 1.0), and self-healing analysis based on the self-healing criteria discussed in Section 3.2. At 400 K in Fig. 10(a and b), the strain softening was not observed in both stress-strain curves. Notably, in the case of GO/vitrimer, the shape of the stress-strain curve is even similar to that of the tensile simulation described in Fig. 9(a) in that the hardening slope is steepened at the strain level above 0.6. Thus we presume that a near-perfect self-healing is achieved on the GO/vitrimer model at 400 K. The snapshots also show that the GO/vitrimer maintains its crosslinked structure at 0.5 strain while the crosslinked structure of the vitrimer begins to collapse at 0.5 strain and ends up with a partial debonding at the strain of 1.0. Based on these analyses, one can conclude that the GO/vitrimer is self-healed completely and the vitrimer is self-healed to some extent but not perfectly. This result is attributed to the simulation temperature which is higher than the T_g of both models. In addition to this, though 400 K is higher than both T_g s, it is 37 K higher than the T_g of GO/vitrimer whereas it is only 17 K higher than the T_g of vitrimer. This might be the reason why the self-healing quality of the GO/vitrimer is better than the vitrimer model.

The GO/vitrimer at 370 K (Fig. 10(c)) does not show any strain softening and the crosslinked structure is intact at 0.5 strain: self-healed successfully. However, in the case of the vitrimer in Fig. 10(d), it is not self-healed since both criteria are not achieved; the stress-strain curve softens, a large debonding is observed at 0.5 strain, and it is nearly divided into two pieces at 1.0 strain. The opposite result in self-healing performance is also directly related to the simulation temperature because it is higher than the T_g of GO/vitrimer and lower than that of vitrimer. Considering the self-healing performance of the vitrimer has been completely changed as we lowered the temperature below the T_g, we can conclude that our MD simulations are capable of describing the change of the self-healing performance around the T_g.

At 300 K in Fig. 10(e and f), both cases are not self-healed well as the stress-strain curves soften. However, there is a difference in self-healing quality. The GO/vitrimer maintains its crosslinked structure to some extent at 0.5 strain whereas the vitrimer is nearly divided into two pieces at the same strain level. Therefore, the self-healing performance of the GO/vitrimer is better than the vitrimer even at the room temperature which is lower than both T_g s.

To sum up, at all three simulation temperatures, the GO/vitrimer is better self-healed than the vitrimer. The major reason for this outcome is the T_g reduction of nanocomposites. As the filler is embedded, the vdW excluded volume emerges at the poor interface between the filler and the matrix [47]. This volume increases the mobility of nearby molecules and finally provokes active bond exchange reactions. However, this is only an analysis based on macroscale properties. An atomistic investigation is needed for detailed explanations.

3.4. Atomistic investigation on the enhanced self-healing performance

We counted new disulfide bonds that emerged during the BER loop through the data files taken out while the self-healing simulation is running. Fig. 11(a) shows the percentage of these new disulfide bonds as the loop count "*a*" increases from 1 to 10 (5ns in timescale). Regardless of the model type and temperature, the number of the new disulfide bonds increases as the BER loop count increases since the BER algorithm implements a successive bond break/creation. Also, as the temperature increases (in the order of dot, dash-dot, and solid line), the percentage of the new disulfide bonds increases in both GO/vitrimer and vitrimer models. This is because as the temperature increases, the probability for a reactive sulfur atom to form a new bond with another sulfur atom increases since their mobility is enhanced.

Comparing the GO/vitrimer with the vitrimer, it is clear that the number of new disulfide bonds in GO/vitrimer is significantly higher than the vitrimer. The black lines are always above the blue lines regardless of the type (dot, dash-dot, and solid line). Especially, in the case of GO/vitrimer at 400 K shown in Fig. 11(a), more than 90% of the disulfide bonds are the new ones that did not exist before the BER simulation. For this reason, we could observe almost the same shape of stress-strain curve in Fig. 10(a) compared to the tensile simulation in Fig. 9(a). This result manifests the enhanced molecular mobility induced by the emergence of the vdW excluded volume and the following T_g

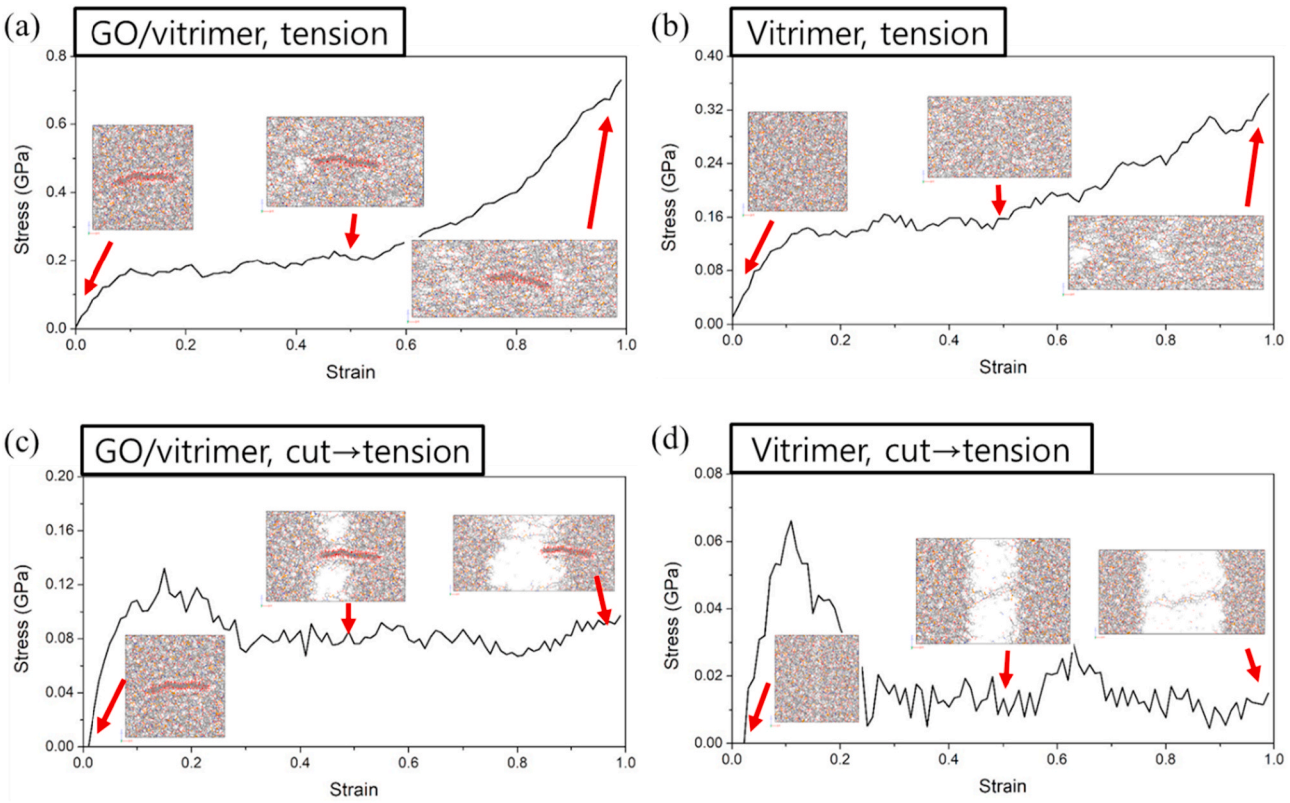

Fig. 9. Control group. Stress-strain curves and snapshots at engineering strains of 0, 0.5, and 1.0 of (a) GO/vitrimer, tension, (b) vitrimer, tension, (c) GO/vitrimer, cut-tension, and (d) vitrimer, cut-tension. (Color online). (For interpretation of the references to color in this figure legend, the reader is referred to the Web version of this article.)

reduction takes a crucial role in generating new disulfide bonds during the BER simulation. Since these bonds are the decisive factor of the self-healing performance and quality, one can conclude that a better self-healing can be achieved by adding the GO into the vitrimer.

Similar results can be obtained from the new-disulfide-bond count in the self-healing region and the interphase. Fig. 11(b) shows the number of new disulfide bonds in the self-healing region defined as 6 Å-thick-region at the cross-section (inset in Fig. 11(b)) when the BER is finished (at "a" = 10, 5 ns). The number of new disulfide bonds decreases as the temperature decreases since the reaction rate is dependent on the temperature. Moreover, at every temperature, a larger number of new disulfide bonds emerge in GO/vitrimer. The same tendency is also found in Fig. 11(c) where the number of new disulfide bonds is counted at the interphase region of GO/vitrimer (characterized in Fig. 8). Because the vitrimer models have no interphase, the values in the graph are adopted as the equivalent number of new disulfide bonds in the 17 Å-thick region, that is, 17/60 of the total number of new disulfide bonds. It is clear that more number of new disulfide bonds are created in the interphase, compared with the bulk matrix phase. These results are the strong evidence in the atomistic perspective that the bond exchange reaction is more active in the GO/vitrimer than the vitrimer, and therefore, the GO/vitrimer exhibits better self-healing performance and quality.

It is worth mentioning that the enhancement in self-healing performance and the bond exchange reaction is expected to take place in other nanofiller/vitrimer systems since the T_g reduction is observed in other nanocomposites such as silica/epoxy and CNT/epoxy systems [46,47]. Further experimental studies and simulations are needed for general nanofiller and vitrimer nanocomposite systems.

4. Conclusions

In this study, we conducted rigorous MD simulations to verify a recent finding that the healing performance of a vitrimer can be enhanced by adding graphene oxide (GO) nanofillers [22] and suggest atomistic elucidation of this phenomenon. We generated realistic MD models for disulfide vitrimers and GO/vitrimer nanocomposites, and devised a disulfide-type BER algorithm to realize the bond exchange chemistry in MD simulations. From the direct comparison of self-healing simulations between GO/vitrimer and vitrimer models conducted at three different temperatures (400 K: higher than T_g of both models, 370 K: higher than T_g of GO/vitrimer but lower than T_g of vitrimer, and 300 K: lower than T_g of both models), we demonstrated two findings. First, a discernible self-healing takes place above the T_g of the material, which is analogous to the experimental results of various vitrimers. This means the proposed BER algorithm consisting of successive bond breaking and creation is adequate for modeling the dynamic covalent bond exchange chemistry in MD simulations. Second, at all three temperatures, the GO/vitrimer models were better self-healed than vitrimer models, which is attributed to the reduced T_g of GO/vitrimer. To suggest an elaborate explanation in the atomic scale, we counted new disulfide bonds that emerged during the BER loop and found a consistent increase in the number of new disulfide bonds at all different temperatures in the case of GO/vitrimer. This is strong evidence that adding GO into the vitrimer can actually increase the dynamic bond exchange reaction.

It is interesting to note that the T_g reduction in polymeric nanocomposites is a general phenomenon observed in various filler/matrix compositions. Therefore, we foresee the findings of this study might be observed from different nanofiller/vitrimer composites. In the future, we will investigate the filler effect of vitrimer nanocomposites in experimental and computational studies.

5. Data availability

The datasets generated during and/or analyzed during the current

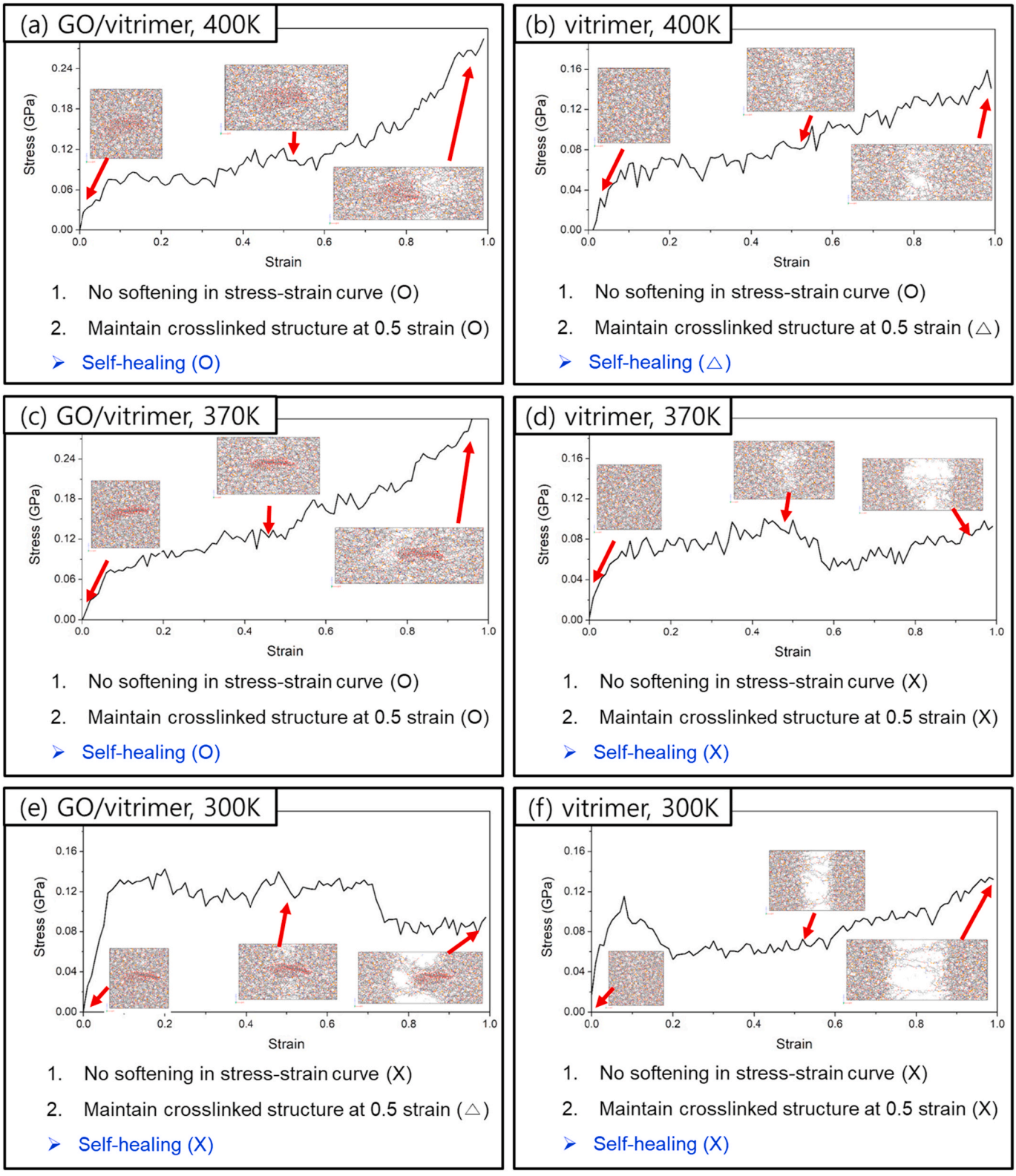

Fig. 10. Self-healing simulation results. Stress-strain curves and snapshots at engineering strains of 0, 0.5, and 1.0 are given with an analysis based on the self-healing performance criteria. (a) GO/vitrimer, 400 K, (b) vitrimer, 400 K, (c) GO/vitrimer, 370 K, (d) vitrimer, 370 K, (e) GO/vitrimer, 300 K, and (f) vitrimer, 300 K. (Color online). (For interpretation of the references to color in this figure legend, the reader is referred to the Web version of this article.)

study are available from the corresponding author on reasonable request.

CRediT authorship contribution statement

Chanwook Park: Formal analysis, Data curation, Investigation, Writing - original draft, Data curation, Visualization, Software.

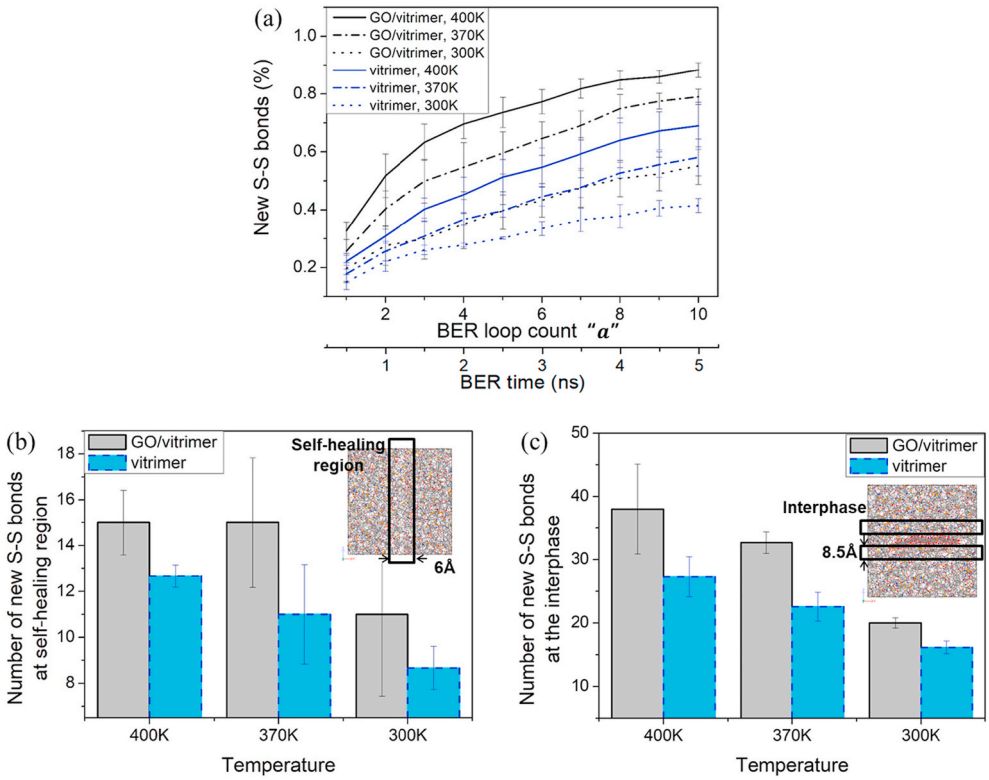

Fig. 11. (a) Percentage of new disulfide bonds as the BER loop count "a" increases. (b–c) Number of new disulfide bonds at the end or the BER loop in the self-healing region (b) and the interphase (c). Insets illustrate the regions of interest. The values are averaged from three different models and the error bar denotes the standard deviation. (Color online). (For interpretation of the references to color in this figure legend, the reader is referred to the Web version of this article.)

Geonwoo Kim: Resources, Validation. **Jiwon Jung:** Software, Methodology. **Balaji Krishnakumar:** Validation. **Sravendra Rana:** Writing - review & editing. **Gun Jin Yun:** Supervision, Writing - review & editing, Project administration, Funding acquisition, Investigation.

Declaration of competing interest

The authors declare that they have no known competing financial interests or personal relationships that could have appeared to influence the work reported in this paper.

Acknowledgments

This work was supported by Creative-Pioneering Researchers Program through Seoul National University (SNU) and National Research Foundation of Korea (NRF) grant funded by the Korea government (MSIP) (2020R1A2B5B01001899) and the Institute of Engineering Research at Seoul National University. Authors are grateful for their support.

Appendix A. Supplementary data

Supplementary data to this article can be found online at https://doi.org/10.1016/j.polymer.2020.122862.

References

[1] D. Montarnal, et al., Silica-like malleable materials from permanent organic networks, Science 334 (6058) (2011) 965–968.
[2] M. Capelot, et al., Metal-catalyzed transesterification for healing and assembling of thermosets, J. Am. Chem. Soc. 134 (18) (2012) 7664–7667.
[3] J.P. Brutman, P.A. Delgado, M.A. Hillmyer, Polylactide vitrimers, ACS Macro Lett. 3 (7) (2014) 607–610.
[4] M. Capelot, et al., Catalytic control of the vitrimer glass transition, ACS Macro Lett. 1 (7) (2012) 789–792.
[5] F.I. Altuna, C.E. Hoppe, R.J. Williams, Epoxy vitrimers with a covalently bonded tertiary amine as catalyst of the transesterification reaction, Eur. Polym. J. 113 (2019) 297–304.
[6] B. Hendriks, et al., Poly (thioether) vitrimers via transalkylation of trialkylsulfonium salts, ACS Macro Lett. 6 (9) (2017) 930–934.
[7] W. Denissen, et al., Vinylogous urethane vitrimers, Adv. Funct. Mater. 25 (16) (2015) 2451–2457.
[8] J. Canadell, H. Goossens, B. Klumperman, Self-healing materials based on disulfide links, Macromolecules 44 (8) (2011) 2536–2541.
[9] C. Luo, M. Kröger, J.-U. Sommer, Molecular dynamics simulations of polymer crystallization under confinement: entanglement effect, Polymer 109 (2017) 71–84.
[10] B. Krishnakumar, et al., Vitrimers: associative dynamic covalent adaptive networks in thermoset polymers, Chem. Eng. J. (2019) 123820.
[11] P. Taynton, et al., Heat-or water-driven Malleability in a highly recyclable covalent network polymer, Adv. Mater. 26 (23) (2014) 3938–3942.
[12] P. Taynton, et al., Repairable woven carbon fiber composites with full recyclability enabled by malleable polyimine networks, Adv. Mater. 28 (15) (2016) 2904–2909.
[13] K. Urdl, et al., Self-healing of densely crosslinked thermoset polymers—a critical review, Prog. Org. Coating 104 (2017) 232–249.
[14] A. Cohades, et al., Progress in self-healing fiber-reinforced polymer composites, Advanced Materials Interfaces 5 (17) (2018) 1800177.
[15] I. Azcune, I. Odriozola, Aromatic disulfide crosslinks in polymer systems: self-healing, reprocessability, recyclability and more, Eur. Polym. J. 84 (2016) 147–160.
[16] W. Post, et al., Healing of a glass fibre reinforced composite with a disulphide containing organic-inorganic epoxy matrix, Compos. Sci. Technol. 152 (2017) 85–93.
[17] K. Yu, et al., Carbon fiber reinforced thermoset composite with near 100% recyclability, Adv. Funct. Mater. 26 (33) (2016) 6098–6106.
[18] Q. Shi, et al., Solvent assisted pressure-free surface welding and reprocessing of malleable epoxy polymers, Macromolecules 49 (15) (2016) 5527–5537.
[19] Y. Yuan, et al., Multiply fully recyclable carbon fibre reinforced heat-resistant covalent thermosetting advanced composites, Nat. Commun. 8 (1) (2017) 1–11.
[20] Y. Sun, et al., A molecular dynamics study of decomposition of covalent adaptable networks in organic solvent, Polymer 180 (2019) 121702.
[21] A.l. Legrand, C. Soulié-Ziakovic, Silica–epoxy vitrimer nanocomposites, Macromolecules 49 (16) (2016) 5893–5902.
[22] B. Krishnakumar, et al., Catalyst free self-healable vitrimer/graphene oxide nanocomposites, Compos. B Eng. (2019) 107647.
[23] K. Balaji, et al., Disulfide exchange assisted self-healing epoxy/PDMS/graphene oxide nanocomposites, Nanoscale Advances 2 (7) (2020) 2726–2730.

[24] S. Plimpton, Fast parallel algorithms for short-range molecular dynamics, J. Comput. Phys. 117 (1) (1995) 1–19.
[25] H. Sun, et al., An ab initio CFF93 all-atom force field for polycarbonates, J. Am. Chem. Soc. 116 (7) (1994) 2978–2987.
[26] M. Hu, P. Keblinski, P.K. Schelling, Kapitza conductance of silicon–amorphous polyethylene interfaces by molecular dynamics simulations, Phys. Rev. B 79 (10) (2009) 104305.
[27] C. Park, J. Jung, G.J. Yun, Thermomechanical properties of mineralized nitrogen-doped carbon nanotube/polymer nanocomposites by molecular dynamics simulations, Compos. B Eng. 161 (2019) 639–650.
[28] F. Zhu, C. Park, G. Jin Yun, An extended Mori-Tanaka micromechanics model for wavy CNT nanocomposites with interface damage, Mech. Adv. Mater. Struct. (2019) 1–13.
[29] R. Rahman, A. Haque, Molecular modeling of crosslinked graphene–epoxy nanocomposites for characterization of elastic constants and interfacial properties, Compos. B Eng. 54 (2013) 353–364.
[30] J. Jung, C. Park, G.J. Yun, Free radical polymerization simulation and molecular entanglement effect on large deformation behavior, Eur. Polym. J. 114 (2019) 223–233.
[31] R.W. Hockney, J.W. Eastwood, Computer Simulation Using Particles, crc Press, 1988.
[32] W.G. Hoover, Canonical dynamics: equilibrium phase-space distributions, Phys. Rev. 31 (3) (1985) 1695.
[33] W.G. Hoover, Constant-pressure equations of motion, Phys. Rev. 34 (3) (1986) 2499.
[34] A. Stukowski, Visualization and analysis of atomistic simulation data with OVITO–the Open Visualization Tool, Model. Simulat. Mater. Sci. Eng. 18 (1) (2009) 15012.
[35] C. Park, G.J. Yun, Characterization of interfacial properties of graphene-reinforced polymer nanocomposites by molecular dynamics-shear deformation model, J. Appl. Mech. 85 (9) (2018) 91007.
[36] Y. Luo, et al., Structures and properties of alkanethiol-modified graphene oxide/solution-polymerized styrene butadiene rubber composites: click chemistry and molecular dynamics simulation, Compos. Sci. Technol. 161 (2018) 32–38.
[37] D.R. Dreyer, et al., The chemistry of graphene oxide, Chem. Soc. Rev. 39 (1) (2010) 228–240.
[38] F. Sciortino, Three-body potential for simulating bond swaps in molecular dynamics, The European Physical Journal E 40 (1) (2017) 3.
[39] L. Rovigatti, et al., Self-dynamics and collective swap-driven dynamics in a particle model for vitrimers, Macromolecules 51 (3) (2018) 1232–1241.
[40] H. Yang, et al., A molecular dynamics study of bond exchange reactions in covalent adaptable networks, Soft Matter 11 (31) (2015) 6305–6317.
[41] H. Yang, et al., Molecular dynamics studying on welding behavior in thermosetting polymers due to bond exchange reactions, RSC Adv. 6 (27) (2016) 22476–22487.
[42] C. Park, et al., Multiscale micromorphic theory and simulation with Co-existing molecular and continuum time scales, in: AIAA Scitech 2020 Forum, 2020.
[43] C. Park, J. Jung, G.J. Yun, Multiscale micromorphic theory compatible with MD simulations in both time-scale and length-scale, Int. J. Plast. (2020) 102680.
[44] W. Denissen, J.M. Winne, F.E. Du Prez, Vitrimers: permanent organic networks with glass-like fluidity, Chem. Sci. 7 (1) (2016) 30–38.
[45] K.S. Khare, F. Khabaz, R. Khare, Effect of carbon nanotube functionalization on mechanical and thermal properties of cross-linked epoxy-carbon nanotube nanocomposites: role of strengthening the interfacial interactions, ACS Appl. Mater. Interfaces 6 (9) (2014) 6098–6110.
[46] K.S. Khare, R. Khare, Effect of carbon nanotube dispersion on glass transition in cross-linked epoxy–carbon nanotube nanocomposites: role of interfacial interactions, J. Phys. Chem. B 117 (24) (2013) 7444–7454.
[47] Z. Wang, et al., Effect of interfacial bonding on interphase properties in SiO2/epoxy nanocomposite: a molecular dynamics simulation study, ACS Appl. Mater. Interfaces 8 (11) (2016) 7499–7508.